

● *Technical Note*

INTERFACIAL RHEOLOGICAL PROPERTIES OF CONTRAST MICROBUBBLE TARGESTAR P AS A FUNCTION OF AMBIENT PRESSURE

KRISHNA N. KUMAR and KAUSIK SARKAR

Department of Mechanical and Aerospace Engineering, The George Washington University, Washington, DC 20052, USA

(Received 4 September 2015; revised 4 November 2015; in final form 18 November 2015)

Abstract—In this Technical Note, we determine the interfacial rheological parameters of the encapsulation of the contrast agent Targestar P using ultrasound attenuation. The characteristic parameters are obtained according to two interfacial rheological models. The properties—surface dilatational elasticity (0.09 ± 0.01 N/m) and surface dilatational viscosity ($8 \pm 0.1E-9$ N·s/m)—are found to be of similar magnitude for both models. Contrast microbubbles experience different ambient pressure in different organs. We also measure these parameters as functions of ambient pressure using attenuation measured at different overpressures (0, 100 and 200 mm Hg). For each value of ambient hydrostatic pressure, we determine the rheological properties, accounting for changes in the size distribution caused by the pressure change. We discuss different models of size distribution change under overpressure: pure adiabatic compression or gas exchange with surrounding medium. The dilatational surface elasticity and viscosity are found to increase with increasing ambient pressure. (E-mail: sarkar@gwu.edu) © 2016 World Federation for Ultrasound in Medicine & Biology.

Key Words: Contrast agents, Interfacial rheology, Encapsulation, Shell, Pressure estimation, Bubble dynamics, Attenuation, Gas diffusion.

INTRODUCTION

Use of lipid-, protein- or polymer-coated microbubbles, such as Optison (GE Healthcare, Oslo, Norway), Sonazoid (GE Healthcare), Definity (Lantheus Imaging, North Billerica, MA, USA), Sonovue (Bracco, Milan, Italy), Targestar (Targeson, San Diego, CA, USA), has led to significant enhancement of the quality of ultrasound imaging (Goldberg et al. 2001; Nahire et al. 2013; 2014; Paul et al. 2014). All these microbubbles differ in size and coating and require careful characterization. Unlike Targestar, the others mentioned have been approved for clinical use in the United States or Europe and have been characterized using controlled *in vitro* acoustic experiments determining the mechanical properties of the coating, for example, Definity (Goertz et al. 2007), Optison (Chatterjee and Sarkar 2003), Sonazoid (Hoff 2001; Paul et al. 2010; Sarkar et al. 2005) and Sonovue (Gorce et al. 2000). In contrast, Targestar has not been similarly characterized. Here, we measure the mechanical properties of Targestar contrast agent under different

ambient hydrostatic pressures using *in vitro* broadband attenuation.

Targestar microbubbles have a perfluorobutane (PFB) gas core encapsulated by a layer of phospholipids (Shekhar et al. 2014) and have been investigated for applications in high frequency subharmonic imaging (Shekhar and Doyley 2011; 2012; 2013; Shekhar et al. 2013) and molecular imaging (Knowles et al. 2012; Saini et al. 2011; Wang et al. 2012; Warram et al. 2011). Targestar SA, Targestar P, Targestar HF and Visistar are a few available variants of this microbubble, each having different applications such as perfusion, labeling and targeting. Here, we describe our investigation of Targestar P agent, a non-targeted perfusion contrast agent designed to enhance and quantify blood flow.

Contrast agents experience widely different pressures in different organs: 5–10 mm Hg in portal vein (D'amico et al. 1995), 8–20 mm Hg in pulmonary artery (Simonneau et al. 2009) and 100–140 mm Hg in left ventricle (systolic) (Lawes et al. 2004). This motivates us to measure the properties of Targestar P under different ambient pressures in the range 0–200 mm Hg. Previously, Hoff (2001) investigated the stability of encapsulated microbubbles under enhanced ambient pressure through attenuation measurement. Recently, we performed a

Address correspondence to: Kausik Sarkar, The George Washington University, 800 22nd Street NW, Suite 3000, Washington, DC 20052, USA. E-mail: sarkar@gwu.edu

detailed characterization of Definity microbubbles, determining pressure-dependent shell properties using attenuation measured at different pressures (Kumar and Sarkar 2015). In this note, a similar procedure is followed for Targestar.

We used ultrasound attenuation through a suspension of contrast agent Targestar under different ambient pressures to determine the interfacial rheological properties of the encapsulation using two different models: the strain-softening exponential elasticity model (EEM) (Paul et al. 2010) and the Marmottant model (Marmottant et al. 2005).

METHODS

Contrast agent

Targestar P agent was procured from Targeson, delivered in suspension form in glass vials with a perfluorobutane headspace. The agent was stored at 4°C in accordance with the product specification. Before use, the vial was shaken very gently two or three times to mix the contents, and then 10 μL was extracted from the vial using a syringe and mixed in 100 mL of standard phosphate-buffered saline (PBS) solution. The resulting dispersion has $2.54 \times 10^5/\text{mL}$ bubbles (according to the information supplied by the vendor).

Estimation of encapsulation parameters using attenuation

In our earlier publications (Chatterjee and Sarkar 2003; Kumar and Sarkar 2015; Paul et al. 2010; 2013; Sarkar et al. 2005), we described in detail the procedure for determining the encapsulation properties of an encapsulation based on different models using attenuation data. Here, attenuation was measured in an airtight setup that can control the ambient pressure with an accuracy of 0.07 kPa (Fig. 1a, b) using an unfocused broadband transducer (Olympus NDT, Waltham, MA, USA) with a central frequency of 3.5 MHz (6-dB bandwidth: 2.5–4.99 MHz). It was excited by a pulser/receiver (Model 5800, Panametrics-NDT, Waltham, MA, USA) to produce a broadband pulse with a pulse repetition frequency of 100 Hz with a peak amplitude of 35 kPa at 3.5 MHz, low enough so that the acoustic propagation

oscilloscope (Model TDS 2012; Tektronix, Beaverton, OR, USA) to observe the signal in real time. A pressure gauge (SSI Technologies, Janesville, WI, USA) was used to measure the static pressure of the chamber. Signals were acquired from the oscilloscope using LabView (National Instruments, Austin, TX, USA) software. Fifty voltage–time radiofrequency traces were acquired in an averaging mode (64 sequences are used for averaging) and saved. They were transformed to frequency domain and averaged for 50 acquisitions. The frequency-dependent attenuation coefficient was calculated using the expression

$$\alpha(\omega) = 20 \log \left(\frac{\overline{V}_{\text{ref}}(\omega)}{\overline{V}_{\text{sig}}(\omega)} \right) / d, \quad (1)$$

where $\overline{V}_{\text{ref}}(\omega)$ is the averaged response in the frequency domain without any contrast agent in the medium, $\overline{V}_{\text{sig}}(\omega)$ is the averaged response in the frequency domain microbubbles suspended in the medium and $d = 10$ cm is the total path traveled by the pulse before it is being received by the transducer. Theoretically an expression for attenuation is obtained using a linearized version of the modified Rayleigh–Plesset equation with an effective surface tension $\gamma(R)$ and interfacial dilatational viscosity $\kappa^s(R)$ (Paul et al. 2010) for bubble radius $R(t)$:

$$\rho \left(R\ddot{R} + \frac{3}{2}\dot{R}^2 \right) = P_g \left(1 - 3\kappa \frac{\dot{R}}{c} \right) - 4\mu \frac{\dot{R}}{R} - \frac{4\kappa_s(R)\dot{R}}{R^2} - \frac{2\gamma(R)}{R} - P_0 + P_A \sin \omega t. \quad (2)$$

here, ρ is the density of the liquid; P_g is the gas pressure inside the bubble, which expands with a polytropic coefficient κ ; c is the speed of sound in the liquid, μ is its viscosity; and P_0 is the ambient pressure. Since with oscillations at megahertz frequency Peclet number $\text{Pe} = R_0^2 \omega / D_g \sim 1$ (D_g is the thermal diffusivity; for C_4F_{10} 2.57×10^{-6} m^2/s), we assume an adiabatic behavior for the gas inside ($\kappa = \kappa_{\text{ad}} = 1.07$ for C_4F_{10}). The bubble is responding to an ultrasound wave with amplitude P_A and circular frequency ω . The EEM uses

$$\gamma(R) = \gamma_0 + E^s \beta, \quad \beta = (R/R_E)^2 - 1, \quad E^s = E_0^s \exp(-\alpha^s \beta), \quad \text{and} \quad \kappa^s(R) = \kappa^s \quad (\text{constant}), \quad (3)$$

through the microbubble suspension remains linear (Chatterjee et al. 2005a; 2005b). The pulse traveled a total distance of 10 cm through the contrast agent suspension before being received and fed to the digital

characterizing the encapsulation with a reference surface tension γ_0 , reference dilatational elasticity E_0^s and coefficient α^s . R_E is the stress-free radius. The Marmottant model uses

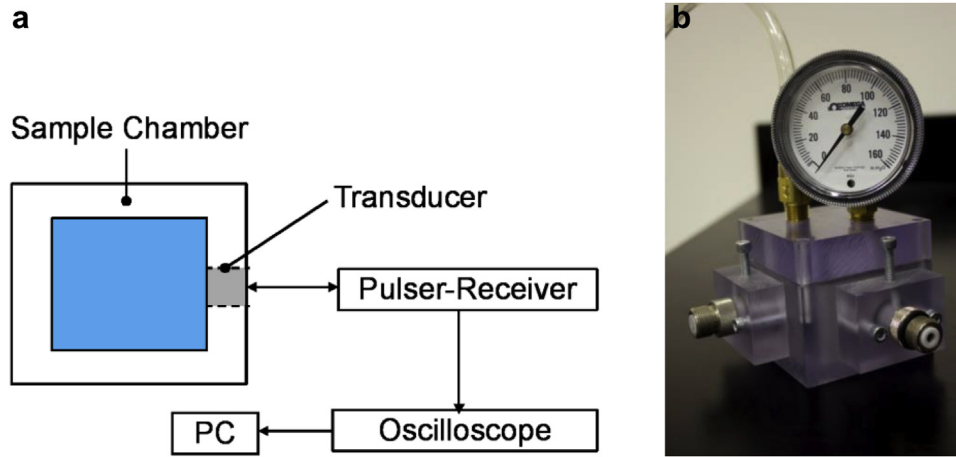


Fig. 1. (a) Schematic of the experimental setup used to measure acoustic attenuation. (b) Airtight chamber. Reprinted with permission from Kumar & Sarkar, J Acoust Soc Am 2015;138:624–634. Copyright 2015, Acoustical Society of America.

$$\gamma(R) = \begin{cases} 0 & \text{for } R \leq R_{\text{buckling}} \\ \chi \left(\frac{R^2}{R_{\text{buckling}}^2} - 1 \right) & \text{for } R_{\text{buckling}} \leq R \leq R_{\text{rupture}} \text{ and } \kappa^s(R) = \kappa^s \text{ (constant),} \\ \gamma_w & \text{for } R \geq R_{\text{rupture}} \end{cases} \quad (4)$$

where χ [same as E^s in (3)] is the elastic modulus of the shell, $R_{\text{buckling}} = R_0 [1 + \gamma(R_0)/\chi]^{-1/2}$ and $R_{\text{rupture}} = R_{\text{buckling}} [1 + \gamma_w/\chi]^{1/2}$. Above R_{rupture} , the bubble is assumed to have a pure air–water interface, and below R_{buckling} , it is in a buckled state, where the effective interfacial tension is zero. Attenuation $\theta(\omega)$ through a suspension of contrast agent is computed as

$$\theta(\omega) = 10 \log e \int_{R_{\text{min}}}^{R_{\text{max}}} \sigma_e(R; \omega) n(R) dR, \quad (5)$$

$$\sigma_e = 4\pi R_0^2 \frac{c\delta}{\omega_0 R_0} \frac{\Omega^2}{[(1 - \Omega^2)^2 + \Omega^2 \delta^2]}, \quad \Omega = \frac{\omega_0}{\omega},$$

where $n(R)dR$ is the number of bubbles per unit volume with radius in the range $(R, R + dR)$, and the range of bubble radii is given by $(R_{\text{min}}, R_{\text{max}})$. The non-dimensional damping term δ is given by

An error function between the measured and modeled attenuation is minimized to find the interfacial rheological parameters, for example, γ , κ^s , E^s , α^s (Sarkar et al. 2005). The bubble count of $2.54 \times 10^5/\text{mL}$ with average bubble diameter of $2.2 \mu\text{m}$ indicates a bubble–bubble separation of ~ 70 diameter. This validates the fundamental assumption underlying the attenuation analysis of no interactions between individual bubbles. The linear dependence of attenuation with bubble concentration has been previously investigated (Sarkar et al. 2005).

Size distribution and changes with ambient pressure

Figure 2 illustrates the size distribution of Targestar microbubbles measured at atmospheric pressure (0 mm Hg of overpressure) provided by the manufacturer. The measurement could not resolve bubbles less than $1 \mu\text{m}$ in diameter. It contains $2.54 \times 10^9/\text{mL}$ bubbles with an

$$\delta = \delta_{\text{liquid}} + \delta_{\text{encapsulation}} + \delta_{\text{radiation}} + \delta_{\text{thermal}} = \frac{4\mu}{\rho\omega_0 R_0^2} + \frac{4\kappa^s}{\rho\omega_0 R_0^3} + \frac{3\kappa P_0}{\rho\omega_0 R_0 c} + \frac{1}{\omega\omega_0} \frac{3P_0}{\rho R_0^2} \text{Im} \left(\frac{1}{\Phi(R_0, \omega)} \right), \quad (6)$$

$$\Phi(R_0, \omega) = \frac{1}{\kappa_{\text{ad}}} \left(1 + \frac{3(\kappa_{\text{ad}} - 1)}{X^2} (X \coth X - 1) \right), \quad X(R_0, \omega) = R_0 \sqrt{\frac{i\omega}{D_g}}$$

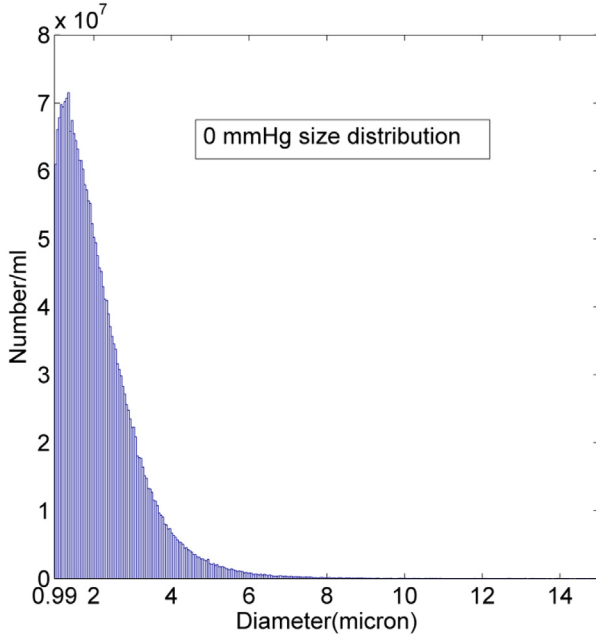


Fig. 2. Size distribution of Targestar P microbubble.

average diameter of 2.2 μm . The size distribution is similar to that obtained by [Shekhar and Doyley \(2012\)](#). As noted above, the dilution in PBS decreases the count to $2.54 \times 10^5/\text{mL}$. Attenuation measured at 0 mm Hg after temporarily subjecting the suspension to 200 mm Hg for 3 min produced a result similar to that obtained without any pressure change, indicating little irreversible destruction of microbubbles under pressure change ([Kumar and Sarkar 2015](#)). An identical conclusion was drawn by [Hoff \(2001\)](#) through similar attenuation measurement. However, microbubbles can reversibly change size with pressure change because of mechanical compression or gas diffusion. A sudden increase in overpressure leads to a transient disequilibrium, which can give rise to gas diffusion from/into the microbubble. Although the air concentration far from the bubble is determined by the saturation level at atmospheric pressure p_{atm} , the concentration near the bubble interface is higher in equilibrium with the gas inside the bubble. We have previously developed a mathematical model for gas diffusion from encapsulated microbubbles ([Borden and Longo 2002](#); [Epstein and Plesset 1950](#); [Katiyar et al. 2009](#); [Sarkar et al. 2009](#)). Note that gas diffusion critically depends on the gas permeability through the encapsulation. The encapsulating shell is definitely more permeable to air than PFB because of the larger size of PFB molecules. We will assume that within the experimental time, because of its larger size and lower solubility, there is negligible diffusion of PFB, and the size change is affected only by air diffusion—below we refer to this as model A1. However for comparison, we also consider two other models. In model A2, we completely ignore

gas diffusion and assume adiabatic compression under pressure, as was done by others ([Frinking et al. 2010](#); [Tremblay-Darveau et al. 2014](#)). The third case, model A3, considers a completely air-filled microbubble. Note that even with a small amount of PFB diffusion, eventually all PFB is replaced by air ([Paul et al. 2010](#); [Sarkar et al. 2005](#)). Although, within the time of the experiment, it is unlikely that such a state will be reached, we consider it just for comparison.

With the initial condition of, $\dot{R} = \ddot{R} = 0$, eqn (2) reduces to an equation for the initial gas pressure inside a bubble of initial radius R_0 :

$$P_{g0} = \frac{2\gamma(R_0)}{R_0} + P_0, \quad P_0 = p_{\text{atm}} + p_{\text{over}}. \quad (7)$$

Model A1: Bubble retains PFB and air diffuses out. Here we assume PFB content remains unchanged. At any instant, the net gas pressure inside the microbubble described by eqn (7), comprise air and PFB at partial pressures p_A and p_F ,

$$P_{g0} = p_A + p_F = \frac{2\gamma(R)}{R_0} + p_{\text{atm}} + p_{\text{over}}. \quad (8)$$

at each overpressure level, the dissolved air concentration far from the bubble is $C_A(\infty)$, and in the liquid adjacent to the microbubble, containing air at pressure p_A , it is $C_A(R)$. These are given by Henry's law:

$$C_A(\infty) = L_A \frac{p_{\text{atm}}}{R_G T}, \quad C_A(R) = L_A \frac{p_A}{R_G T}. \quad (9)$$

L_A is the Ostwald coefficient relating dissolved concentration to adjacent gas concentration. R_G and T are the universal gas constant and the temperature, respectively. After overpressure change, gas exchange and accompanying diffusion lead to a new equilibrium $C_A(\infty) = C_A(R)$ obtaining $p_A = p_{\text{atm}}$. At zero overpressure with initial radius R_0^0 , eqn (8) gives rise to

$$p_F = \frac{n_F R_G T}{\frac{4}{3}\pi(R_0^0)^3} = \frac{2\gamma(R_0^0)}{R_0^0} = \frac{2\gamma_0}{R_0^0}. \quad (10)$$

the number of moles n_F of PFB remains constant. Unlike in our previous publications, here we cannot assume $\gamma(R_0^0) = 0$. Instead, we assume $R_E = R_0^0$, that is, a stress-free condition, which leads to the second equality in (10). At non-zero overpressure, one obtains

$$p_F = \frac{n_F R_G T}{\frac{4}{3}\pi(R_0)^3} = \frac{2\gamma(R_0)}{R_0} + p_{\text{over}} \quad \text{or} \quad (11)$$

$$\frac{2\gamma_0}{R_0^0} \left(\frac{R_0^0}{R_0}\right)^3 = \frac{2}{R_0} \left(\gamma_0 + E^s \left(\left(\frac{R_0}{R_0^0}\right)^2 - 1 \right) \right) + p_{\text{over}}.$$

solving eqn (11) results in R_0 at new overpressure p_{over} . $\gamma(R_0)$ is expressed as in (3) using values of γ_0 and E^s obtained at zero overpressure as an approximation. This approximation is used in all three approaches. After interfacial rheological properties are estimated at non-zero overpressure, they are then used to iteratively improve this approximation to find little difference in results.

Model A2: No gas exchange. From eqn (7), at $p_{\text{over}}=0$, the initial gas pressure as $P_{g0}^0 = p_{\text{atm}}$, where $\gamma(R_0^0)$ is assumed to be zero at initial radius R_0^0 . Assuming an adiabatic process for the gas inside the bubble, the initial bubble radius would change from R_0^0 to R_0 when subjected to non-zero overpressure according to

$$\frac{2}{R_0} \left(\gamma_0 + E^s \left(\left(\frac{R_0}{R_E} \right)^2 - 1 \right) \right) + p_{\text{atm}} + p_{\text{over}} = p_{\text{atm}} \left(\frac{R_0^0}{R_0} \right)^{3\kappa} \quad (12)$$

at non-zero p_{over} yields the new radius.

Model A3: Air-filled bubble exchanging air with medium. Here we assume that all PFB has diffused out, leaving air-filled microbubbles. At $p_{\text{over}}=0$, assumption of a steady bubble warrants $\gamma(R_0^0) = 0$. At other overpressures,

$$\frac{2\gamma(R_0)}{R_0} + p_{\text{over}} = 0 \quad \text{or} \quad \frac{2}{R_0} \left(\gamma_0 + E^s \left(\left(\frac{R_0}{R_E} \right)^2 - 1 \right) \right) + p_{\text{over}} = 0, \quad (13)$$

which is solved to obtain R_0 .

Figure 3 illustrates the predicted change in radius when bubbles are subjected to 100 and 200 mm Hg overpressures using all three models. Model A2, which assumes no gas exchange, results in the least decrease in radius. Model A3, which assumes purely air bubbles, gives rise to the maximum radius change. They give rise to different modifications of the size distribution illustrated in Figure 2. They are all used to obtain the rheological properties.

RESULTS AND DISCUSSION

Rheological parameters at different overpressures

In Figure 4 we plot the measured attenuation curves at three different overpressures. The attenuation decreases with the increase in ambient overpressure to a frequency of 3.75 MHz, beyond which attenuation increases with increasing overpressure. Also plotted are the fitted curves used to obtain the rheological parameters according to the EEM model. The fitting is similar to that for the MM model. The properties are listed in Table 1 for EEM

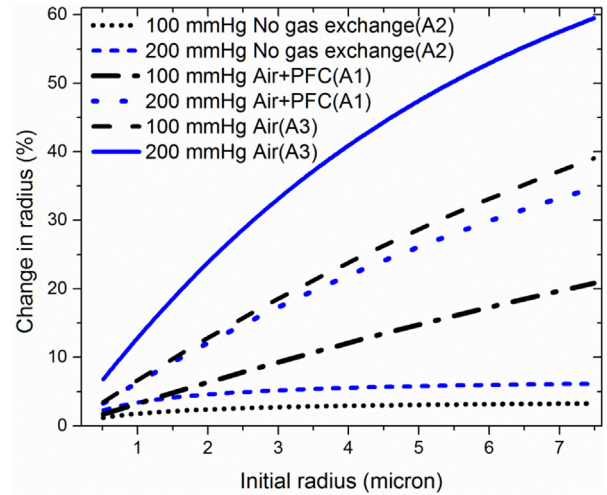


Fig. 3. Percentage changes in radius over values at atmospheric pressure, at two different ambient overpressures, according to three different models (A1, A2 and A3) of bubble size change.

and Table 2 for MM. First note the similarity between the MM and EEM models for all pressures and different approaches to calculation of radius change, that is, similar values of κ^s for both models and similar values of E^s (EEM) and χ (MM). The similarity in property values across different models indicates the robustness of the approach. Also note that the linear theory underlying attenuation computation linearizes the bubble dynamics, leading to very similar forms for both models.

We first note that the surface dilatational elasticity E^s value of Targestar P microbubbles is rather low, 0.09 N/m, compared with the values for other lipid-coated microbubbles: Sonazoid (~ 0.5 N/m) (Sarkar et al. 2005), SonoVue (~ 0.55 N/m) (van der Meer et al.

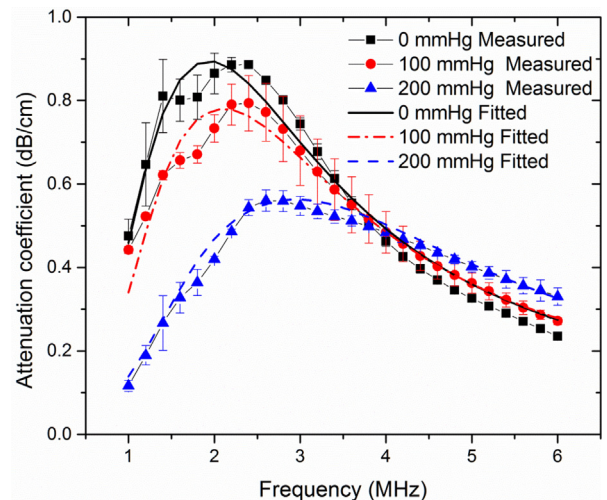


Fig. 4. Measured frequency-dependent attenuation curves at different ambient overpressures along with exponential elasticity model predictions using model A1 for radius change.

Table 1. Rheological parameters of Targestar P bubbles according to the exponential elasticity model using three different approaches to calculation of the radius change under overpressure

| Approach used | Encapsulation parameter | 0 mm Hg | 100 mm Hg | 200 mm Hg |
|---|---|-------------------|-------------------|-------------------|
| Perfluorobutane content constant, air diffuses (A1) | $\kappa^s(\times 10^{-9} \text{N}\cdot\text{s}/\text{m})$ | 8.0 ± 0.1 | 8.17 ± 0.3 | 9.3 ± 0.3 |
| | $E_0^s(\text{N}/\text{m})$ | 0.09 ± 0.01 | 0.085 ± 0.02 | 0.19 ± 0.01 |
| | α | 1.5 ± 0.5 | 2 ± 0.5 | 2 ± 0.5 |
| | $\gamma_0(\text{N}/\text{m})$ | 0.01 ± 0.005 | 0.001 ± 0.001 | 0.007 ± 0.002 |
| No gas exchange, mechanical compression (A2) | $\kappa^s(\times 10^{-9} \text{N}\cdot\text{s}/\text{m})$ | 8.0 ± 0.1 | 8.68 ± 0.1 | 10.56 ± 0.1 |
| | $E_0^s(\text{N}/\text{m})$ | 0.09 ± 0.01 | 0.11 ± 0.005 | 0.31 ± 0.005 |
| | α | 1.5 ± 0.5 | 1 ± 0.5 | 1 ± 0.5 |
| | $\gamma_0(\text{N}/\text{m})$ | 0.01 ± 0.005 | 0.01 ± 0.005 | 0.01 ± 0.005 |
| Air-filled bubble exchanging air with medium (A3) | $\kappa^s(\times 10^{-9} \text{N}\cdot\text{s}/\text{m})$ | 8.22 ± 0.2 | 7.3 ± 0.2 | 6.55 ± 0.3 |
| | $E_0^s(\text{N}/\text{m})$ | 0.035 ± 0.005 | 0.022 ± 0.005 | 0.032 ± 0.003 |
| | α | 1 ± 0.5 | 1 ± 0.5 | 1 ± 0.5 |
| | $\gamma_0(\text{N}/\text{m})$ | 0.01 ± 0.01 | 0.001 ± 0.001 | 0.001 ± 0.001 |

2007), Definity (0.5–2.5 N/m) (Faez et al. 2011; Helfield and Goertz 2013; Kumar and Sarkar 2015; Raymond et al. 2014) and Micromarker (3–5 N/m) (Helfield and Goertz 2013). The surface dilatational viscosity value $\kappa^s \sim 8 \times 10^{-9} \text{N}\cdot\text{s}/\text{m}$ is similar to that of SonoVue ($5 \times 10^{-9} \text{N}\cdot\text{s}/\text{m}$) (van der Meer et al. 2007) and smaller than that of Sonazoid ($1.2 \times 10^{-8} \text{N}\cdot\text{s}/\text{m}$) (Sarkar et al. 2005) or Definity's ($4 \times 10^{-8} \text{N}\cdot\text{s}/\text{m}$) (Kumar and Sarkar 2015). Note that the attenuation (measured with a transducer with nominal central frequency 3.5 MHz) is limited here to the frequency range below ~ 6 MHz (Fig. 4). The shell properties listed here are therefore representative of this frequency range and may substantially differ outside, specifically above this range. Also note that contrast agents exhibit considerable variability from batch to batch. The properties estimated here are based on experiments performed on the particular vials of contrast microbubbles. The relatively low value of the surface elasticity leads to a low resonance frequency—from the attenuation curve, the size averaged resonance at 0 mm Hg is ~ 2.2 MHz.

Figure 5 plots the variations in surface dilatational elasticity (Fig. 5a) and surface dilatational viscosity (Fig. 5b) with increasing pressure. We first look at the model of our choice A1, where we assume that PFB content remains constant and the bubble shrinks because of air egress. We find that both E^s and κ^s increase with

increasing ambient pressure. Note that the resonance frequency of a microbubble increases with increasing E^s . Therefore, the increasing trend of E^s with overpressure can be related to the rightward shift of the peak of the attenuation in Figure 4. For a monodisperse suspension of microbubbles, the peak of the attenuation curve occurs at the resonance frequency. For a polydisperse suspension, the peak represents a weighted average resonance frequency of the suspension. The weighted resonance frequency in Figure 4 increases from 2.2 MHz at 0 mm Hg to 2.4 MHz at 100 mm Hg and 2.6 MHz at 200 mm Hg. In *in vitro* attenuation measurement, Hoff (2001) found that for lipid-coated Sonazoid agent, the resonance frequency (peak in the attenuation) increases with overpressure increase—similar to the observation here for Targestar—but for polymeric microbubbles, it decreases with overpressure. The opposite trend for polymeric microbubbles was surmised to be caused by curling/buckling of the stiff shell. Recently, Tremblay-Darveau et al. (2014) saw a similar increase in resonance frequency in backscattered signals from phospholipid-coated agent under overpressure. They too ascribed the observation to pressure-induced shell buckling. When one assumes no gas exchange, but just mechanical compression under ambient pressure increase (curve for A2), the variation is similar but higher in magnitude. Note that this assumption, as noted before, has been used previously (Frinking

Table 2. Rheological parameters of Targestar P bubbles according to the Marmottant model using three different approaches to calculation of the radius change under overpressure

| Approach used | Encapsulation parameter | 0 mm Hg | 100 mm Hg | 200 mm Hg |
|---|---|-------------------|-------------------|-------------------|
| Perfluorobutane content constant, air diffuses (A1) | $\kappa^s(\times 10^{-9} \text{N}\cdot\text{s}/\text{m})$ | 8.32 ± 0.2 | 8.37 ± 0.3 | 9.14 ± 0.3 |
| | $\chi(\text{N}/\text{m})$ | 0.092 ± 0.01 | 0.078 ± 0.008 | 0.21 ± 0.01 |
| No gas exchange, mechanical compression (A2) | $\kappa^s(\times 10^{-9} \text{N}\cdot\text{s}/\text{m})$ | 8.28 ± 0.2 | 8.94 ± 0.1 | 10.83 ± 0.4 |
| | $\chi(\text{N}/\text{m})$ | 0.089 ± 0.008 | 0.10 ± 0.005 | 0.316 ± 0.005 |
| Air-filled bubble exchanging air with medium (A3) | $\kappa^s(\times 10^{-9} \text{N}\cdot\text{s}/\text{m})$ | 8.65 ± 0.2 | 7.46 ± 0.4 | 6.79 ± 0.2 |
| | $\chi(\text{N}/\text{m})$ | 0.05 ± 0.005 | 0.015 ± 0.003 | 0.044 ± 0.003 |

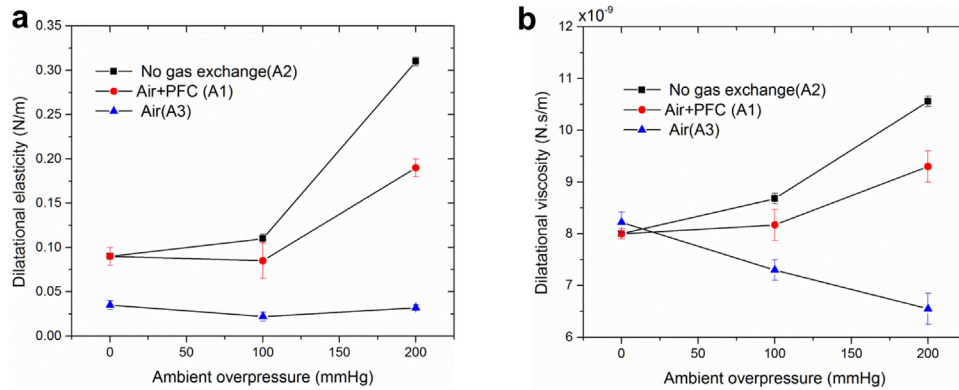


Fig. 5. Variation in surface dilatational elasticity (a) and surface dilatational viscosity (b) with change in ambient pressure according to the exponential elasticity model.

et al. 2010, Tremblay-Darveau et al. 2014). The property values for this assumption are the highest, arising from the minimum relative change in size distribution under model A2 in Figure 4. The low value of surface elasticity is responsible for the relatively large decrease in radius under pressure increase. Finally, when the unlikely case of a fully air-filled microbubble (model A3) is assumed, very little change in E^s and a decreasing trend in κ^s are observed with increasing overpressure. We parenthetically note that this wide variance in results underscores the importance of choosing the right model and the limitation of the technique in the absence of a right size distribution.

CONCLUSIONS

We used broadband attenuation of ultrasound measured at different hydrostatic pressures to estimate shell properties of Targestar contrast agent. Two interfacial rheological models, the strain-softening exponential elasticity model (EEM) and the Marmottant model (MM), were applied to the attenuation data. The bubble size decrease with static pressure increase was accounted for using different gas diffusion models. Different models of encapsulation gave rise to similar shell property values, but different assumptions about gas diffusion results in different pressure dependence of interfacial properties. Dilatational elasticity increased from ~ 0.1 N/m at 0 mm Hg to ~ 0.2 – 0.3 N/m at 200 mm Hg, whereas dilatational viscosity increased from $\sim 8 \times 10^{-9}$ to 10×10^{-9} N·s/m at the same pressure values. The increases in these properties with increasing pressure arise from the bubble size decrease, which causes contraction of the encapsulation and enhanced association of the lipid molecules.

Acknowledgments—This work is partially supported by NSF Grants CBET-1205322 and DMR-1239105 and the GWU Katzen Cancer Research Center Innovative Cancer Pilot Research Award. We also

gratefully acknowledge Targeson and Dr. Joshua Rychack for the contrast microbubbles used here.

REFERENCES

- Borden MA, Longo ML. Dissolution behavior of lipid monolayer-coated, air-filled microbubbles: Effect of lipid hydrophobic chain length. *Langmuir* 2002;18:9225–9233.
- Chatterjee D, Jain P, Sarkar K. Ultrasound-mediated destruction of contrast microbubbles used for medical imaging and drug delivery. *Phys Fluids* 2005a;17:100603.
- Chatterjee D, Sarkar K, Jain P, Schreppler NE. On the suitability of broadband attenuation measurement for characterizing contrast microbubbles. *Ultrasound Med Biol* 2005b;31:781–786.
- Chatterjee D, Sarkar KA. Newtonian rheological model for the interface of microbubble contrast agents. *Ultrasound Med Biol* 2003;29:1749–1757.
- D'amico G, Pagliaro L, Bosch J. The treatment of portal hypertension: A meta-analytic review. *Hepatology* 1995;22:332–354.
- Epstein PS, Plesset MS. On the stability of gas bubbles in liquid–gas solutions. *J Chem Phys* 1950;18:1505–1509.
- Faez T, Goertz D, De Jong N. Characterization of Definity (TM) ultrasound contrast agent at frequency range of 5–15 MHz. *Ultrasound Med Biol* 2011;37:338–342.
- Frinking PJ, Gaud E, Brochot J, Arditi M. Subharmonic scattering of phospholipid-shell microbubbles at low acoustic pressure amplitudes. *IEEE Trans Ultrason Ferroelectr Freq Control* 2010;57:1762.
- Goertz DE, de Jong N, van der Steen AFW. Attenuation and size distribution measurements of Definity (TM) and manipulated Definity (TM) populations. *Ultrasound Med Biol* 2007;33:1376–1388.
- Goldberg BB, Raichlen JS, Forsberg F. *Ultrasound contrast agents: Basic principles and clinical applications*. London: Martin Dunitz; 2001.
- Gorce JM, Arditi M, Schneider M. Influence of bubble size distribution on the echogenicity of ultrasound contrast agents: A study of SonoVue (TM). *Investig Radiol* 2000;35:661–671.
- Helfield BL, Goertz DE. Nonlinear resonance behavior and linear shell estimates for Definity (TM) and MicroMarker (TM) assessed with acoustic microbubble spectroscopy. *J Acoust Soc Am* 2013;133:1158–1168.
- Hoff L. *Acoustic characterization of contrast agents for medical ultrasound imaging*. Norwell, MA: Kluwer Academic, 2001.
- Katiyar A, Sarkar K, Jain P. Effects of encapsulation elasticity on the stability of an encapsulated microbubble. *J Colloid Interface Sci* 2009;336:519–525.
- Knowles JA, Heath CH, Saini R, Umphrey H, Warram J, Hoyt K, Rosenthal EL. Molecular targeting of ultrasonographic contrast agent for detection of head and neck squamous cell carcinoma. *Arch Otolaryngol Head Neck Surg* 2012;138:662–668.

- Kumar KN, Sarkar K. Effects of ambient hydrostatic pressure on the material properties of the encapsulation of an ultrasound contrast microbubble. *J Acoust Soc Am* 2015;138:624–634.
- Lawes CM, Vander Hoorn S, Law MR, Elliott P, MacMahon S, Rodgers A. High blood pressure. Comparative quantification of health risks: Global and regional burden of disease attributable to selected major risk factors. Geneva: World Health Organization; 2004. p. 281–390.
- Marmottant P, van der Meer S, Emmer M, Versluis M, de Jong N, Hilgenfeldt S, Lohse D. A model for large amplitude oscillations of coated bubbles accounting for buckling and rupture. *J Acoust Soc Am* 2005;118:3499–3505.
- Nahire R, Haldar MK, Paul S, Ambre AH, Meghnani V, Layek B, Katti KS, Gange KN, Singh J, Sarkar K, Mallik S. Multifunctional polymersomes for cytosolic delivery of gemcitabine and doxorubicin to cancer cells. *Biomaterials* 2014;35:6482–6497.
- Nahire R, Haldar MK, Paul S, Mergoum A, Ambre AH, Katti KS, Gange KN, Srivastava DK, Sarkar K, Mallik S. Polymer-coated echogenic lipid nanoparticles with dual release triggers. *Biomacromolecules* 2013;14:841–853.
- Paul S, Katiyar A, Sarkar K, Chatterjee D, Shi WT, Forsberg F. Material characterization of the encapsulation of an ultrasound contrast microbubble and its subharmonic response: Strain-softening interfacial elasticity model. *J Acoust Soc Am* 2010;127:3846–3857.
- Paul S, Nahire R, Mallik S, Sarkar K. Encapsulated microbubbles and echogenic liposomes for contrast ultrasound imaging and targeted drug delivery. *Comput Mech* 2014;53:413–435.
- Paul S, Russakow D, Rodgers T, Sarkar K, Cochran M, Wheatley MA. Determination of the interfacial rheological properties of a poly(DL-lactic acid)-encapsulated contrast agent using in vitro attenuation and scattering. *Ultrasound Med Biol* 2013;39:1277–1291.
- Raymond JL, Haworth KJ, Bader KB, Radhakrishnan K, Griffin JK, Huang SL, McPherson DD, Holland CK. Broadband attenuation measurements of phospholipid-shelled ultrasound contrast agents. *Ultrasound Med Biol* 2014;40:410–421.
- Saini R, Warram JM, Sorace AG, Umphrey H, Zinn KR, Hoyt K. Model system using controlled receptor expression for evaluating targeted ultrasound contrast agents. *Ultrasound Med Biol* 2011;37:1306–1313.
- Sarkar K, Katiyar A, Jain P. Growth and dissolution of an encapsulated contrast microbubble. *Ultrasound Med Biol* 2009;35:1385–1396.
- Sarkar K, Shi WT, Chatterjee D, Forsberg F. Characterization of ultrasound contrast microbubbles using in vitro experiments and viscous and viscoelastic interface models for encapsulation. *J Acoust Soc Am* 2005;118:539–550.
- Shekhar H, Awuor I, Thomas K, Rychak JJ, Doyley MM. The delayed onset of subharmonic and ultraharmonic emissions from a phospholipid-shelled microbubble contrast agent. *Ultrasound Med Biol* 2014;40:727–738.
- Shekhar H, Doyley MM. A coded excitation technique for the functional imaging of coronary atherosclerosis using ultrasound contrast agents. *J Acoust Soc Am* 2011;129:2610.
- Shekhar H, Doyley MM. Improving the sensitivity of high-frequency subharmonic imaging with coded excitation: A feasibility study. *Med Phys* 2012;39:2049–2060.
- Shekhar H, Doyley MM. The response of phospholipid-encapsulated microbubbles to chirp-coded excitation: Implications for high-frequency nonlinear imaging. *J Acoust Soc Am* 2013;133:3145–3158.
- Shekhar H, Rychak JJ, Doyley MM. Modifying the size distribution of microbubble contrast agents for high-frequency subharmonic imaging. *Med Phys* 2013;40:082903.
- Simonneau G, Robbins IM, Beghetti M, Channick RN, Delcroix M, Denton CP, Elliott CG, Gaine SP, Gladwin MT, Jing ZC. Updated clinical classification of pulmonary hypertension. *J Am Coll Cardiol* 2009;54:S43–S54.
- Tremblay-Darveau C, Williams R, Burns PN. Measuring absolute blood pressure using microbubbles. *Ultrasound Med Biol* 2014;40:775–787.
- Van der Meer SM, Dollet B, Voormolen MM, Chin CT, Bouakaz A, de Jong N, Versluis M, Lohse D. Microbubble spectroscopy of ultrasound contrast agents. *J Acoust Soc Am* 2007;121:648–656.
- Wang X, Hagemeyer CE, Hohmann JD, Leitner E, Armstrong PC, Jia F, Olschewski M, Needles A, Peter K, Ahrens I. Novel single-chain antibody-targeted microbubbles for molecular ultrasound imaging of thrombosis validation of a unique noninvasive method for rapid and sensitive detection of thrombi and monitoring of success or failure of thrombolysis in mice. *Circulation* 2012;125:3117–3126.
- Warram JM, Sorace AG, Saini R, Umphrey HR, Zinn KR, Hoyt K. A triple-targeted ultrasound contrast agent provides improved localization to tumor vasculature. *J Ultrasound Med* 2011;30:921–931.